Steering the Selectivity of Electrochemical CO_2 Reduction in Acidic Media

Zhanyou Xu[a], Mingzi Sun[b], Zhongshuo Zhang[a], Yi Xie[a], Hongshuai Hou[c], Xiaobo Ji[c], Tianfei Liu[d], Bolong Huang[b]* and Ying Wang[a]*

[a] Z. Xu, Z. Zhang, Y. Xie, Prof. Y. Wang
Department of Chemistry
Chinese University of Hong Kong
Ma Lin building, Shatin, N.T. HK SAR, China
E-mail: ying.b.wang@cuhk.edu.hk
http://ywanggroup.com/

[b] M. Sun, Prof. B. Huang
Department of Applied Biology and Chemical Technology
The Hong Kong Polytechnic University
Hung Hom, Kowloon, Hong Kong SAR, China
E-mail: bhuang@polyu.edu.hk
https://www.polyu.edu.hk/abct/people/academic-staff/dr-huang-bolong/

[c] Prof. H. Hou, Prof. X. Ji
Key Laboratory of Hunan Province for Chemical Power Source,
College of Chemistry and Chemical Engineering,
Central South University, Changsha 410083, China

[d] Prof. T. Liu
State Key Laboratory of Elemento-organic Chemistry,
Department of Chemistry,
Nankai University, 300071, Tianjin, China.

Supporting information for this article is given via a link at the end of the document.

Abstract: Improving carbon utilization efficiency is the key to developing next-generation electrolysers for CO_2 reduction reaction (CO_2RR). The current CO_2RR electrolyser relies on the use of neutral/alkaline media to suppress the competitive hydrogen production and improve the activity of CO_2RR. However, the produced carbonate/bicarbonate leads to severe carbon loss. Performing CO_2RR in acidic media can suppress the carbonate formation while hydrogen production is the major issue. By chronopotentiometry in flow electrolyser, we found that the activity of acidic CO_2RR can be well tuned through electrolyte optimization. DFT calculation suggests that this results from the change of local electronic structure of Cu catalyst by surface adsorbed alkali metal ions. Electrolytes with high content of K^+ promote the overall CO_2RR activity, especially multi-carbon production in acidic media. CH_4 is the dominant product in Na^+ only electrolyte on Cu, with a Faradaic efficiency of 48% at 220 mA cm^{-2} in pH = 2 solution.

Introduction

Renewable-electricity-powered CO_2 conversion is a promising approach to convert CO_2 into value-added chemical feedstocks and fuels.[1] Tremendous efforts have been made to develop efficient CO_2 electrolysers.[2] Commercial relevant current densities are achieved for CO_2RR in alkaline and neutral media. The commonly used alkaline condition is suggested to suppress the competitive hydrogen evolution reaction (HER) and promote further reduced species, like ethylene and ethanol.[2a, c, 3] Gewirth and co-workers obtained highly efficient C_2H_4 production (faradaic efficiency (FE) = 72% and C_2H_4 partial current density = 312 mA cm^{-2}) using 1 M KOH as electrolyte.[4] Wang and co-workers have achieved a high selectivity of CO_2-to-C_{2+} (FE = 80%) at a current density of 1.6 A cm^{-2} in 1 M KOH electrolyte in flow cell.[5]

While significant progress is realized in the alkaline/neutral CO_2RR, further practical application is limited by the low carbon utilization efficiency under these conditions. It is inhibited by a fundamental acid-base reaction, which leads to undesired carbonate formation (Eq. 1 and left panel in Fig. 1).[6]

$$CO_2 + OH^- \rightarrow HCO_3^-/CO_3^{2-} + H_2O \quad (1)$$

The locally alkaline chemical environment at the electrode surface shifts the reaction equilibria at Eq. 1 to the formation of carbonate with increased applied current density and number of electrons transferred.[6-7] The formed carbonate will be subsequently transported to the anode chamber through the anion exchange membrane, leading to severe carbon loss and low carbon utilization efficiency. Around 60% of CO_2 is found in the anode gas outlet resulting in high energy costs for gas separation.[8] The techno-economic analysis (TEA) by Sargent et al. suggested that CO_2 regeneration from carbonate takes up to 23% of the capital cost for CO_2 electrolysers[6, 9]

Hence, addressing the issue of carbonate formation is the key to the industrial implementation of CO_2RR. Acidic media, especially for pH < 4, with CO_2 as the primary carbon species, can effectively avoid carbon loss for high carbon utilization efficiency. The formed carbonate at the interface can be converted back to CO_2 at bulk solution (right panel in Fig. 1). While acidic CO_2RR seems to be ideal, the sluggish kinetics and poor selectivity under such conditions are huge challenges. The reaction rate of HER is about a few magnitudes faster in the acidic condition than that in the

alkaline media.[2a] Chan found that low pH is not beneficial for further reduced species from CO_2 based on DFT calculation.[10] This agrees with a few recent experimental works that CO and formate are the main products in acidic CO_2RR.[11] Thus, suppressing the competitive HER and improving the selectivity of CO_2RR towards further reduced species are critical for realizing efficient acidic CO_2RR.

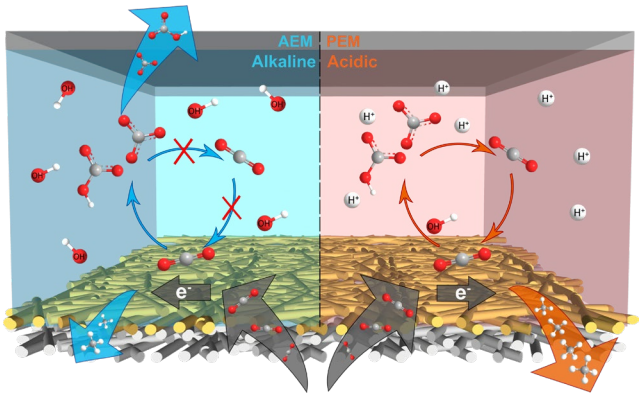

Figure 1. Schematic of CO_2RR and carbon transport under alkaline (blue) and acidic (red) conditions. C, O and H atoms are illustrated as grey, red and white balls, respectively.

Electrolyte, behaving as an electrochemical "second coordination sphere," influences the selectivity and activity of inner-sphere electrochemical reaction through manipulating local environments such as pH and local electrical field.[12] Recent works have shown that electrolyte engineering can steer the activity of CO_2RR by up to a few orders of magnitude.[12b, c] Koper and co-workers demonstrated the necessity of cation for CO_2RR through the intermediate stabilization by large size cation, like Cs^+.[13] Sargent and Burdyny both reported enhancement of CO_2RR by K^+ cation in a flow cell reactor and bipolar membrane electrode assemblies.[14] DFT calculations suggested that CO_2RR intermediates can be stabilized by specific adsorption of cations, with a similar trend for different cations.[15]

Based on the recent advances in electrolyte optimization, we further explored the impact of electrolytes on the development of acidic CO_2RR electrolysers. We were able to control the activity and selectivity of CO_2RR over HER by tuning the ratio of Na^+:K^+ in the electrolyte. The HER is suppressed in the electrolyte with higher K^+ content on Ag and Cu at pH = 2. Additionally, in the Na^+ only electrolyte, the dominant product of CO_2RR is CH_4 with a faradaic efficiency of 48% and a partial current density of 106 mA cm^{-2}. This is a significant improvement in CO_2-to-CH_4 in acidic media. Density functional theory (DFT) calculation suggested that the local electronic structure can be modulated through different coverage of K^+ and Na^+. Higher electron density was found on Cu surface with higher K^+ coverage leading to enhancement of C_{2+} while Cu surface covered with Na^+ is beneficial for C_1, such as CH_4 production.

Results and Discussion

Cu and Ag, the state-of-the-art CO_2RR catalysts with distinct products distribution, are chosen as the targeted catalysts. Since our research focuses on electrolyte engineering, we adopt benchmark polycrystalline Cu-PTFE and Ag-PTFE for studies. The Cu and Ag catalysts were coated on polytetrafluoroethylene (PTFE) porous fibers through E-beam evaporation. The as-prepared Cu-PTFE and Ag-PTFE were characterized by scanning electron microscope (SEM, Fig. 2a-d) and X-ray powder diffraction (XRD, Fig. 2e and f). Both Cu and Ag are homogeneously distributed on the PTFE fiber. The XRD spectrum confirmed the characteristic peaks of polycrystalline Cu and Ag, which are consistent with previous works of Cu-PTFE and Ag-PTFE.[2c, 16]

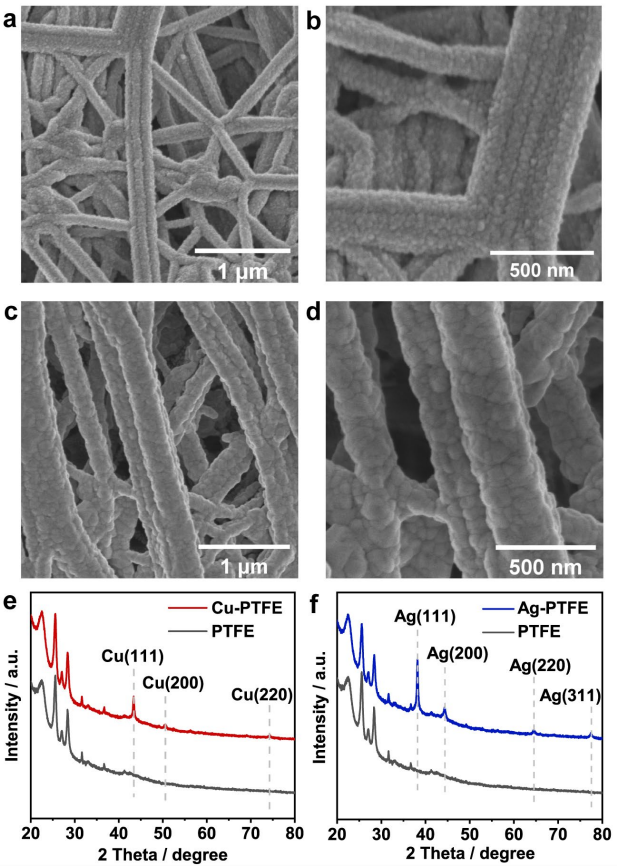

Figure 2. Characterizations of Cu-PTFE and Ag-PTFE GDE. SEM images of Cu-PTFE at (a) low and (b) high magnification. SEM images of Ag-PTFE at (c) low and (d) high magnification. XRD spectrum of (e) Cu-PTFE and (f) Ag-PTFE compared with bare PTFE substrate

We conducted CO_2RR in acidic solution at commercial relevant current density (> 200 mA cm^{-2}) on Cu-PTFE and Ag-PTFE to investigate the electrolyte effect. All the electrolytes were at pH = 2 with a constant ionic strength of 3 for the studies at high current density. A dependence of FE_{CO2RR} to the ratio of Na^+:K^+ on Cu-PTFE and Ag-PTFE was observed. The faradaic efficiency of CO_2RR increased from (62 ± 2)% to (84 ± 2)% on Cu-PTFE in Na^+ only electrolyte to K^+ only electrolyte (Fig. 3a). The same effect was observed on Ag-PTFE (Fig. 3a), where the ratio of FE_{CO2RR}:FE_{HER} increased from 0.4 ± 0.05 to 3.7 ± 1.7 in Na^+ electrolyte to K^+ electrolyte.

The ratio of Na^+:K^+ is also found to influence the product distribution. As shown in Fig. 3b, single selectivity of CO_2 to CH_4 (FE_{CH4} = (48 ± 3)% and FE_{H2} = (39 ± 3)%) is achieved in Na^+ only electrolyte on Cu-PTFE. This leads to a j_{CH4} = 106 mA cm^{-2}, which

is among the best CO_2-to-CH_4 in acidic media (Table S3 and S4). CH_4 is the dominant product from CO_2RR at different current densities from 140 to 260 mA cm^{-2} (Fig. S1) in Na^+ only electrolyte. In contrast, the introduction of K^+ favors the C_2 pathway (Fig. 3c). When ratio of Na^+:K^+ decreases to 1:1, C_{2+} products (FE_{C2+} = 61%) become dominant with the lowest value of FE_{CH4}:FE_{C2+} = 0.16 at 140 mA cm^{-2}. Different electrolytes can steer the competition between CH_4 and C_2 pathway on copper within a wide range of current densities.

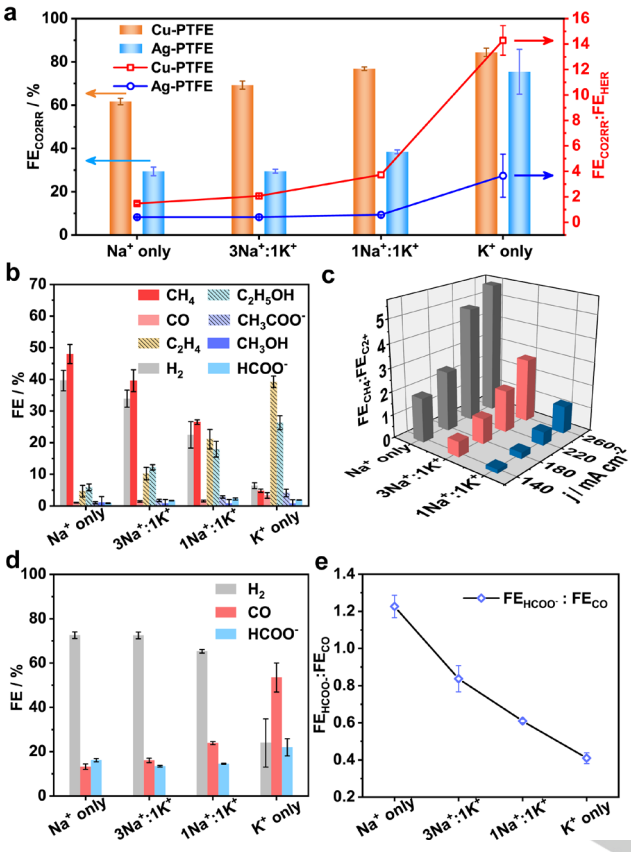

Figure 3. (a) Total FE of CO_2RR and FE_{CO2RR}:FE_{HER} on Cu-PTFE and Ag-PTFE in different electrolytes at 220 mA cm^{-2}. (b) Product distribution and (c) FE_{CH4}:FE_{C2+} in CO_2RR on Cu-PTFE with different electrolytes at different current densities. (d) Product distribution and (e) FE_{HCOO^-}:FE_{CO} on Ag-PTFE in different electrolytes at a current density of 220 mA cm^{-2}. The values are means, and error bars in a, b, d and e indicate SD (n = 3 replicates).

On Ag-PTFE, Na^+ only electrolyte leads to the dominant HER (FE = (73 ± 2)%) while the addition of K^+ is able to suppress HER for promoting CO production. For K^+ only electrolyte, HER is suppressed (FE = (24 ± 11)%), and the FE is (53 ± 7)% for CO (Fig. 3d). The ratio of FE_{HCOO^-}:FE_{CO} decreased from 1.2 ± 0.06 in Na^+ only solution to 0.4 ± 0.03 in K^+ only solution, suggesting the promotion of CO over $HCOO^-$ by addition of K^+ (Fig. 3e). The interfacial electrical field induced by cations was reported to influence the intermediates through dipole interaction. Cations with larger ionic radius (e.g. K^+) tend to stabilize intermediates with larger dipole moments, especially for O-terminated species (e.g. CO*, which is the key intermediate for CO production).[12b, 15b] The improved CO production with an increased ratio of K^+ to Na^+ may attribute to the favored stabilization of CO* over HCOO* by K^+.[12b] The well tuning of CO_2RR selectivity on Ag-PTFE reveals the universality of electrolyte effects on CO_2RR catalysts beyond Cu. No noticeable structural changes were observed in XRD and SEM on Cu-PTFE and Ag-PTFE before and after bulk electrolysis (Fig. S4 and S5), suggesting that electrolyte composition has a significant contribution to the change of product distribution.

We further applied DFT calculations to investigate the electrolyte effect in acidic CO_2RR on Cu surfaces. Based on the experiments, four different electrolyte environments are considered including only Na^+ ions, only K^+ ions, and the mixing ions with Na^+:K^+ ratio of 3:1 and 1:1 on Cu surfaces. The corresponding influences on the surface electronic distributions are distinct with different ions (Fig. 4a-d). It is noted that on the Cu (111) surfaces with only Na^+ ions, the anti-bonding orbital (green isosurface) shows more dominant contributions on the surface. For the Cu (111) surface covered with more K^+ ions, the surface shows stronger contributions of the bonding orbitals, leading to a higher possibility to realize the adsorption of the intermediates by activating more surface Cu sites.

The projected partial density of states (PDOSs) suggested that the overall electronic structure of Cu remains stable as the 3d orbitals have not changed with different cations (Fig. 4e-g). In the meantime, we notice that K-4s orbitals show a slightly downshifting trend than the Na-3s orbitals, which promotes higher electron density near E_F to facilitate efficient electron transfer. Interestingly, we have noticed that the mixing ions have significantly changed the s orbitals in K^+. The K-4s orbitals have exhibited a sharp peak at E_V +2.01 eV, indicating a strong sensitivity to the orbital couplings, while the Na-3s orbitals remain unchanged. These results further confirm that the introduction of sensitive K^+ ions facilitates electron transfer and modulates the surface electronic environments.

From the site-dependent PDOS, we noticed that the surface electrolyte ions slightly downshift the d-band center of surface Cu sites, improving the reduction capability (Fig. 4h). In comparison, the mixing ions lead to a slightly downshifted d-band center compared to the pristine electrolyte. Besides the electronic structures, the energy comparisons also support the experimental results (Fig. 4i). Compared to Na^+ ions, K^+ ions display higher orbital sensitivity and a much stronger preference in binding on Cu surfaces. The competition between HER and CO_2RR is revealed by the binding energy evolutions of CO_2 and proton (Fig. 4j). The proton adsorption on the pristine Cu surface is more energetically favorable than CO_2, supporting the strong HER trend. From Na^+ to $3Na^+$:$1K^+$, the adsorption of the proton has changed from spontaneous to energetically unfavored, which indicates the important role of K^+ in suppressing the competitive HER. When the content of K^+ is further increased, the adsorption of proton has become relatively stable with a very small adsorption energy change (< 0.1 eV) considering the adsorbate-adsorbate interaction with adsorbed CO_2,[17] while the increase of CO_2 binding energy promotes the adsorption of CO_2 and leads to increased CO_2RR activity. For Na^+ covered surface, the proton adsorption is still slightly more preferred than the CO_2 adsorption, leading to the high FE of HER. It is worth noting that the introduction of K^+ ions largely suppresses the HER process due to the much higher energy cost than CO_2RR.

The adsorption of key adsorbates CHO* and OCCO* are important for the formation of CH_4 and C_2H_4, respectively, which show a converse trend (Fig. 4k). As the increase of K^+ ions in the

electrolyte, the adsorption of CHO* becomes much weaker and even becomes energetically unfavored, indicating a suppressed C_1 pathway. The OCCO* adsorptions are less competitive than CHO* on Cu surfaces with high Na^+ concentrations, which leads to the low FE for C_2 products. The competition between C_1 and C_2 products is not only related to the adsorption of key intermediates (CHO* and OCCO*) but also the reaction barriers of the CO_2RR process. We have compared the energy change for both C_1 and C_2 pathways on the four different surfaces (Fig. 4l and 4m) under zero potential. For the C_1 pathways, it is noted that surfaces with high K^+ concentration show the high energy barrier for the formation of CHO*. In comparison, Cu surfaces with high Na^+ concentration are energetically favorable for conversion from CO* to CHO*, leading to a stronger preference for the C_1 products. During the C_1 pathway, the conversion from CHOH* to CH_2OH* is more preferred than the formation of CH*. In addition, we notice that the overall reaction trends of CH_4 formation are strong on Cu surfaces with Na^+ ions and Na^+:K^+ = 3:1. These results have unravelled that the formation of C_1 products is affected by the cations. For the C_2 pathways, the formation of CO dimer through coupling displays the most evident energy barriers, which suggests the rate-determining step (RDS) (Fig. 4m). Such energy barriers increase as the concentration of Na ions, where the large barriers strongly hinder the C_2 pathway on the Cu surfaces with Na^+ ions and Na^+:K^+ = 3:1 coverage. The hydrogenation from OCCO* towards the CHCHO* is energetically favorable for all the surfaces. The formation of CH_3CHO meets higher energy barriers than the formation of CH_2CHOH, which demonstrates the less possibility of acetaldehyde formation, supporting the experimental results. Meanwhile, as the concentration of K^+ ions becomes higher, the formation of C_2H_4 becomes more preferred than C_2H_5OH. Therefore, DFT calculation results have demonstrated the influences of cations in the electrolyte on the selectivity during the CO_2RR.

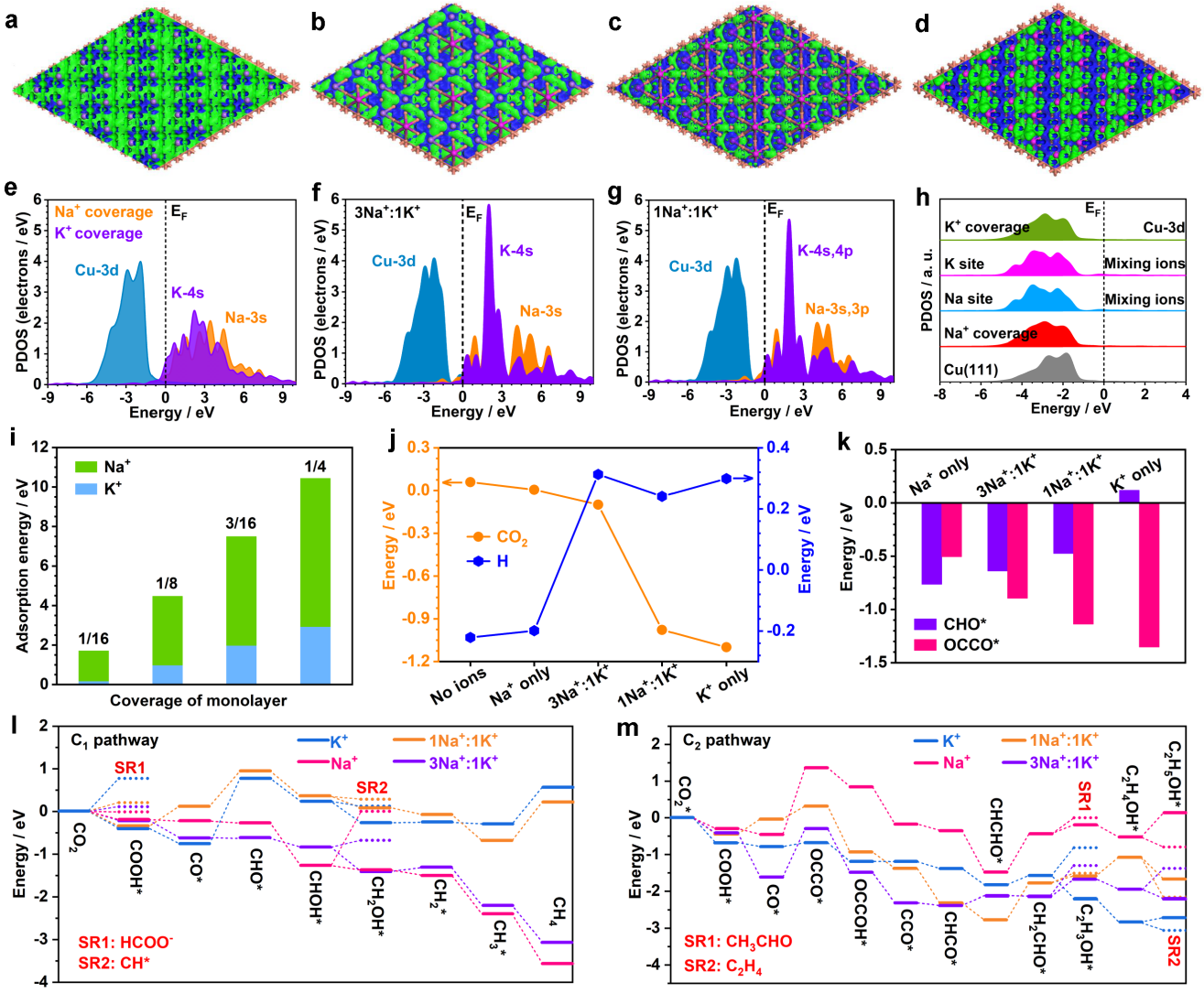

Figure 4. The 3D contour plots of electronic distributions near the Fermi level of (a) Na^+ ion, Na^+/K^+ ions in the ratio of (b) 3:1 and (c) 1:1, and (d) K^+ ion on the Cu surface. Orange balls = Cu, purple balls = Na^+ and pink, blue balls = K^+. Blue isosurface = bonding orbitals and green isosurface = anti-bonding orbitals. The PDOS of Cu surface with (e) pristine Na^+ and pristine K^+ ions, Na^+/K^+ ions in the ratio of (f) 3:1, and (g) 1:1. (h) The site-dependent PDOS of surface Cu with different cations. (i) The energy cost for varying coverage of Na^+ and K^+ ions on the Cu surface. (j) The adsorption energy comparisons for proton and CO_2 on Cu surfaces with different cations. (k) The adsorption energy comparisons of key adsorbates CHO* and OCCO* on Cu surfaces with different cations. (l) The reaction energies of C_1 pathways towards the formation of CH_4. (m) The reaction energies of C_2 pathways towards the formation of C_2H_4. The free energy changes are calculated at 0 V vs reversible hydrogen electrode (RHE).

Conclusion

We investigated the electrolyte effects of CO_2RR in acidic media by varying the ratio of Na^+ to K^+ on Cu and Ag catalysts. The overall CO_2RR FE is 14 and 4 times higher than competitive HER on Cu and Ag in K^+ only solution. On Cu-PTFE, electrolytes with different ratios of Na^+ and K^+ also influence the competition between CH_4 and C_{2+}. CH_4 is the dominant product with a faradaic efficiency of 48% and a partial current density of 106 mA cm^{-2}. This is among the highest CO_2-to-CH_4 in acidic media. DFT calculations suggest that the surface electronic distribution on Cu can be manipulated through cation adsorption. K^+ is found to improve the local electron density at the Cu, enhancing the selectivity and activity of CO_2RR. The modulation of CO_2RR activity and product distribution highlights the role of electrolyte engineering in developing acidic CO_2RR systems.

Experimental Section

Materials and Chemicals

Sodium sulfate (Na_2SO_4, AR, 99%), potassium sulfate (K_2SO_4, ACS) and sulfuric acid (H_2SO_4, AR, 98%) were purchased from commercial suppliers and all the chemical reagents were used as received without any other purification. All aqueous solutions were prepared using deionized water with a resistivity of 18.25 MΩ cm. The polytetrafluoroethylene (PTFE) membrane with an average pore size of 450 nm is purchased from Beijing Zhongxingweiye Instrument Co., Ltd.

Electrode Preparation and Characterizations

Porous PTFE membrane was coated with 90 nm Cu (Cu target, 99.999%) or 100nm Ag (Ag target, 99.999%) by electron-beam evaporation (EB-600, Innovative Vacuum Solution Co., Ltd.) to fabricate Cu-PTFE or Ag-PTFE cathode gas diffusion electrode (GDE), respectively. Scanning electron microscopy (SEM) of all samples were conducted using Hitachi Regulus 8230 scanning electron microscope. X-ray diffraction (XRD) analysis was conducted on Rigaku SmartLab SE X-ray powder diffractometer with Cu-K*α* radiation.

Electrochemical Measurements

All the electrochemical measurements were conducted in an electrochemical flow cell electrolyser with three-electrode configuration. Ag/AgCl electrode (saturated with KCl, IDA) and Pt mesh (30 mm × 15 mm, 99.99%, Gaoss Union) were used as reference and counter electrode, respectively. The as-prepared Cu-PTFE or Ag-PTFE gas diffusion electrode was placed between gas and catholyte chamber. A proton exchange membrane (Nafion 117, Fuel Cell Store) was used to separate catholyte and anolyte chamber. In acidic CO_2RR, the aqueous solution containing different ratio of Na_2SO_4 to K_2SO_4 were used as the electrolyte, which was all adjusted to pH = 2 by H_2SO_4 and the total ionic strength were kept at 3. Detailed compositions of electrolytes used are listed in Supporting Information (Table S1). The catholyte and anolyte were circulated through the cathode and anode chamber at a rate of 7 mL min^{-1} by two peristaltic pumps, respectively. Pure CO_2 gas (Air Products, 99.99%) serving as reactant was continuously fed into the gas chamber at a flow rate of 50 mL min^{-1}. The CO_2RR performance was tested by electrochemical workstation (ZAHNER ZENNIUM pro) using chronopotentiometric method unless otherwise specified. The data of chronopotentiometry are provided in Supporting Information (Fig. S2-3). The potentials vs. Ag/AgCl reference electrode were converted to RHE reference scale using equation:

$$E_{\mathrm{RHE}} = E_{\mathrm{Ag/AgCl}} + 0.197\ \mathrm{V} + 0.0591 \times \mathrm{pH}$$

Products Analysis

Gaseous products were on-line analyzed by gas chromatograph (Ramiin GC 2060) equipped with flame ionization and thermal conductivity detectors. The calibration curves for CO, CH_4, C_2H_4 and H_2 were obtained by injection of certified standard gas samples (Scientific Gas Engineering Co., Ltd.) diluted with pure CO_2. Liquid products were quantified by nuclear magnetic resonance spectrometer (Bruker AVANCE III HD 500) and dimethyl sulfoxide was used as internal standard.

DFT Calculations

To study the effect of electrolyte ions in CO_2RR, DFT calculations have been applied to investigate the electronic structures and energetic trends based on the CASTEP packages. For all the calculations, the generalized gradient approximation (GGA) with Perdew-Burke-Ernzerhof (PBE) is chosen to describe the exchange-correlation energy. In this work, we have set the plane-wave basis cutoff energy to be 380 eV with the ultrasoft pseudopotentials for all the geometry optimizations. The Broyden-Fletcher-Goldfarb-Shannon (BFGS) algorithm has been applied in this work. The coarse quality of k-points is applied for all the energy minimizations. For the Cu surface, we have cleaved from Cu (111) surfaces with six-layered thickness in the 4 × 4 supercell to investigate the effect of cations with 1/4 monolayer adsorption in different electrolytes. Four different electrolytes have been considered in this work with different Na^+:K^+ ratios as 1:0, 3:1, 1:1, 0:1 to match the experimental results. For the energy costs of the cation coverage, we have introduced 1 to 4 cations on the surface as 1/16 to 1/4 monolayer, respectively. We have applied 20 Å vacuum space on the z-axis to guarantee full relaxation. For all the geometry optimizations, the calculations have to satisfy the following convergence criteria that the Hellmann-Feynman forces on the atom should not exceed 0.001 eV $Å^{-1}$, and the total energy difference and the inter-ionic displacement should be less than 5 × 10^{-5} eV $atom^{-1}$ and 0.005 Å, respectively. More details of calculation setup have been supplied in Supporting Information.

Acknowledgements

Z.X., Z.Z., Y.X., and Y.W. acknowledge the support of the Research Grants Council of the Hong Kong Special Administrative Region (project no. 24304920). B.H. acknowledges the support of the National Key R&D Program of China (2021YFA1501101), the Natural Science Foundation of China (Grant No.: NSFC 21771156), and the NSFC/RGC Joint Research Scheme (N_PolyU502/21), and the funding for Projects of Strategic Importance of The Hong Kong Polytechnic University (Project Code: 1-ZE2V).

Keywords: CO_2 Reduction • Electrocatalysis • Electrolyte Engineering • Interfacial Electrochemistry

[1] a) J. A. Martens, A. Bogaerts, N. De Kimpe, P. A. Jacobs, G. B. Marin, K. Rabaey, M. Saeys, S. Verhelst, *ChemSusChem* **2017**, *10*, 1039-1055; b) M. B. Ross, P. De Luna, Y. Li, C.-T. Dinh, D. Kim, P. Yang, E. H. Sargent, *Nat. Catal.* **2019**, *2*, 648-658; c) R. Li, K. Xiang, Z. Peng, Y. Zou, S. Wang, *Adv. Energy Mater.* **2021**, *11*, 2102292.

[2] a) C.-T. Dinh, T. Burdyny, G. Kibria Md, A. Seifitokaldani, M. Gabardo Christine, F. P. García de Arquer, A. Kiani, P. Edwards Jonathan, P. De Luna, S. Bushuyev Oleksandr, C. Zou, R. Quintero-Bermudez, Y. Pang, D. Sinton, E. H. Sargent, *Science* **2018**, *360*, 783-787; b) C. M. Gabardo, C. P. O'Brien, J. P. Edwards, C. McCallum, Y. Xu, C.-T. Dinh, J. Li, E. H. Sargent, D. Sinton, *Joule* **2019**, *3*, 2777-2791; c) C.-T. Dinh, F. P. García de Arquer, D. Sinton, E. H. Sargent, *ACS Energy Lett.* **2018**, *3*, 2835-2840; d) Z. Liu, H. Yang, R. Kutz, R. I. Masel, *J. Electrochem. Soc.* **2018**, *165*, J3371-J3377.

[3] a) M. G. Kibria, C.-T. Dinh, A. Seifitokaldani, P. De Luna, T. Burdyny, R. Quintero-Bermudez, M. B. Ross, O. S. Bushuyev, F. P. García de Arquer, P. Yang, D. Sinton, E. H. Sargent, *Adv. Mater.* **2018**, *30*, 1804867; b) C. M. Gabardo, A. Seifitokaldani, J. P. Edwards, C.-T. Dinh, T. Burdyny, M. G. Kibria, C. P. O'Brien, E. H. Sargent, D. Sinton, *Energy Environ. Sci.* **2018**, *11*, 2531-2539; c) K. J. P. Schouten, Z. Qin, E. Pérez Gallent, M. T. M. Koper, *J. Am. Chem. Soc.* **2012**, *134*, 9864-9867; d) K. J. P. Schouten, E. Pérez Gallent, M. T. M. Koper, *J. Electroanal. Chem.* **2014**, *716*, 53-57; e) J. Li, X. Chang, H. Zhang, A. S. Malkani, M.-j. Cheng, B. Xu, Q. Lu, *Nat. Commun.* **2021**, *12*, 3264; f) L. Wang, S. A. Nitopi, E. Bertheussen, M. Orazov, C. G. Morales-Guio, X. Liu, D. C. Higgins, K. Chan, J. K. Nørskov, C. Hahn, T. F. Jaramillo, *ACS Catal.* **2018**, *8*, 7445-7454.

[4] X. Chen, J. Chen, N. M. Alghoraibi, D. A. Henckel, R. Zhang, U. O. Nwabara, K. E. Madsen, P. J. A. Kenis, S. C. Zimmerman, A. A. Gewirth, *Nat. Catal.* **2021**, *4*, 20-27.

[5] W. Ma, S. Xie, T. Liu, Q. Fan, J. Ye, F. Sun, Z. Jiang, Q. Zhang, J. Cheng, Y. Wang, *Nat. Catal.* **2020**, *3*, 478-487.

[6] J. A. Rabinowitz, M. W. Kanan, *Nat. Commun.* **2020**, *11*, 5231.

[7] U. O. Nwabara, E. R. Cofell, S. Verma, E. Negro, P. J. A. Kenis, *ChemSusChem* **2020**, *13*, 855-875.

[8] M. Ma, E. L. Clark, K. T. Therkildsen, S. Dalsgaard, I. Chorkendorff, B. Seger, *Energy Environ. Sci.* **2020**, *13*, 977-985.

[9] T. Alerte, J. P. Edwards, C. M. Gabardo, C. P. O'Brien, A. Gaona, J. Wicks, A. Obradović, A. Sarkar, S. A. Jaffer, H. L. MacLean, D. Sinton, E. H. Sargent, *ACS Energy Lett.* **2021**, *6*, 4405-4412.

[10] X. Liu, P. Schlexer, J. Xiao, Y. Ji, L. Wang, R. B. Sandberg, M. Tang, K. S. Brown, H. Peng, S. Ringe, C. Hahn, T. F. Jaramillo, J. K. Nørskov, K. Chan, *Nat. Commun.* **2019**, *10*, 32.

[11] a) J. Shen, R. Kortlever, R. Kas, Y. Y. Birdja, O. Diaz-Morales, Y. Kwon, I. Ledezma-Yanez, K. J. P. Schouten, G. Mul, M. T. M. Koper, *Nat. Commun.* **2015**, *6*, 8177; b) Z. Wang, P. Hou, Y. Wang, X. Xiang, P. Kang, *ACS Sustainable Chem. Eng.* **2019**, *7*, 6106-6112; c) D. T. Whipple, E. C. Finke, P. J. A. Kenis, *Electrochem. Solid-State Lett.* **2010**, *13*, B109.

[12] a) G. Marcandalli, M. Villalba, M. T. M. Koper, *Langmuir* **2021**, *37*, 5707-5716; b) J. Resasco, L. D. Chen, E. Clark, C. Tsai, C. Hahn, T. F. Jaramillo, K. Chan, A. T. Bell, *J. Am. Chem. Soc.* **2017**, *139*, 11277-11287; c) S. Ringe, E. L. Clark, J. Resasco, A. Walton, B. Seger, A. T. Bell, K. Chan, *Energy Environ. Sci.* **2019**, *12*, 3001-3014; d) M. R. Singh, Y. Kwon, Y. Lum, J. W. Ager, A. T. Bell, *J. Am. Chem. Soc.* **2016**, *138*, 13006-13012; e) J. Li, F. Cheng, *J. Electrochem.* **2020**, *26*, 474-485.

[13] M. C. O. Monteiro, F. Dattila, B. Hagedoorn, R. García-Muelas, N. López, M. T. M. Koper, *Nat. Catal.* **2021**, *4*, 654-662.

[14] a) E. Huang Jianan, F. Li, A. Ozden, A. Sedighian Rasouli, F. P. García de Arquer, S. Liu, S. Zhang, M. Luo, X. Wang, Y. Lum, Y. Xu, K. Bertens, K. Miao Rui, C.-T. Dinh, D. Sinton, H. Sargent Edward, *Science* **2021**, *372*, 1074-1078; b) K. Yang, M. Li, S. Subramanian, M. A. Blommaert, W. A. Smith, T. Burdyny, *ACS Energy Lett.* **2021**, *6*, 4291-4298.

[15] a) J. N. Mills, I. T. McCrum, M. J. Janik, *PCCP* **2014**, *16*, 13699-13707; b) S. A. Akhade, I. T. McCrum, M. J. Janik, *J. Electrochem. Soc.* **2016**, *163*, F477-F484; c) D. Gao, I. T. McCrum, S. Deo, Y.-W. Choi, F. Scholten, W. Wan, J. G. Chen, M. J. Janik, B. Roldan Cuenya, *ACS Catal.* **2018**, *8*, 10012-10020.

[16] a) X. Wang, A. Xu, F. Li, S.-F. Hung, D.-H. Nam, C. M. Gabardo, Z. Wang, Y. Xu, A. Ozden, A. S. Rasouli, A. H. Ip, D. Sinton, E. H. Sargent, *J. Am. Chem. Soc.* **2020**, *142*, 3525-3531; b) X. Wang, P. Ou, J. Wicks, Y. Xie, Y. Wang, J. Li, J. Tam, D. Ren, J. Y. Howe, Z. Wang, A. Ozden, Y. Z. Finfrock, Y. Xu, Y. Li, A. S. Rasouli, K. Bertens, A. H. Ip, M. Graetzel, D. Sinton, E. H. Sargent, *Nat. Commun.* **2021**, *12*, 3387.

[17] J. J. Mortensen, B. Hammer, J. K. Nørskovi, *Surf. Sci.* **1998**, *414*, 315-329.

Entry for the Table of Contents

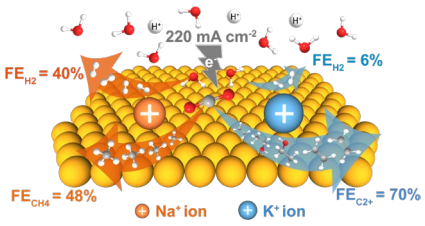

Product distribution of electrochemical CO_2 reduction in acidic media (pH = 2) can be steered by different electrolytes with commercially relevant current density. Different coverage of Na^+ and K^+ ions is found to modulate the local electronic structure on the catalyst surface.

Institute Twitter usernames: @CUHKScience